

Can phenotypic data complement our understanding of antimycobacterial effects for drug combinations?

Frank Kloprogge *, Robert Hammond², Andrew Copas¹, Stephen H. Gillespie² and Oscar Della Pasqua³

¹Institute for Global Health, University College London, London, UK; ²School of Medicine, University of St Andrews, St Andrews, UK;

³Clinical Pharmacology and Therapeutics Group, School of Pharmacy, University College London, London, UK

*Corresponding author. E-mail: f.kloprogge@ucl.ac.uk

Received 5 April 2019; returned 23 June 2019; revised 5 July 2019; accepted 25 July 2019

Objectives: To demonstrate how phenotypic cell viability data can provide insight into antimycobacterial effects for the isoniazid/rifampicin treatment backbone.

Methods: Data from a *Mycobacterium komossense* hollow-fibre infection model comprising a growth control group, rifampicin at three different exposures ($C_{\max} = 0.14, 0.4$ and 1.47 mg/L with $t_{1/2} = 1.57 \text{ h}$ and $\tau = 8 \text{ h}$) and rifampicin plus isoniazid ($C_{\max} \text{ rifampicin} = 0.4 \text{ mg/L}$ and $C_{\max} \text{ isoniazid} = 1.2 \text{ mg/L}$ with $t_{1/2} = 1.57 \text{ h}$ and $\tau = 8 \text{ h}$) were used for this investigation. A non-linear mixed-effects modelling approach was used to fit conventional cfu data, quantified using solid-agar plating. Phenotypic proportions of respiring (alive), respiring but with damaged cell membrane (injured) and 'not respiring' (dead) cells data were quantified using flow cytometry and Sytox Green™ (Sigma-Aldrich, UK) and resazurin sodium salt staining and fitted using a multinomial logistic regression model.

Results: Isoniazid/rifampicin combination therapy displayed a decreasing overall antimicrobial effect with time ($\theta_{Time_{1/2}} = 438 \text{ h}$) on cfu data, in contrast to rifampicin monotherapy where this trend was absent. In the presence of isoniazid a phenotype associated with cell injury was displayed, whereas with rifampicin monotherapy a pattern of phenotypic cell death was observed. Bacterial killing onset time on cfu data correlated negatively ($\theta_{Time_{50}} = 28.9 \text{ h}$, $\theta_{LAG_{RIF_{50}}} = 0.132 \text{ mg/L}$) with rifampicin concentration up to 0.165 mg/L and this coincided with a positive relationship between rifampicin concentration and the probability of phenotypic cell death.

Conclusions: Cell viability data provide structured information on the pharmacodynamic interaction between isoniazid and rifampicin that complements the understanding of the antibacterial effects of this mycobacterial treatment backbone.

Introduction

Many infectious diseases require a combination of antimicrobial drugs to ensure complete pathogen clearance from the body. TB is a good example; it infects 9 million people worldwide each year and TB causes about 1.5 million deaths, which is more than any other infectious disease.¹ Even standard treatment of drug-susceptible TB is complex, with daily oral administration of four antibiotics during the first 2 months, followed by daily oral administration of two antibiotics during a 4 month continuation phase.²

Current treatment evolved from a series of clinical trials over a period of 60 years.³ During this period, drugs and dosing regimens used in randomized controlled trial protocols were empirical with the evidence from one trial being used to plan the next. Consequently, little is known about how such combinations

contribute to bacillary killing even though understanding this phenomenon in a quantitative manner would provide important insights into the activity of existing and novel drug combinations.

Recent efforts to shorten the treatment of drug-susceptible disease have shown that the experimental regimens were not non-inferior compared with standard care^{4,5} and consequently did not lead to changes in treatment guidelines. These findings have prompted further evaluation of the underlying drug interactions and dosing regimens required for combination therapy. In this context, modelling and simulation concepts can provide insight and guidance towards drug and dose selection for treatment combinations for TB treatment. Using pharmacokinetic/pharmacodynamic (PKPD) modelling, for example, one may be able to characterize bacterial clearance using killing rate constants. This is crucial to infer maximum killing, which can subsequently be used to more

accurately predict the time required to achieve complete eradication of the bacterial load.

Predicting the bacillary killing rate remains challenging as treatment of TB requires four antibiotic drugs in different combinations over time.² Moreover, it is important to evaluate the impact of pharmacokinetic characteristics of drug combinations in non-clinical protocols to evaluate total antitubercular activity. Most animal models do not provide exposure profiles that mimic human exposure for known drugs; animal models are also less flexible when evaluating new drug combinations, as exposure ratios change over time due to species-specific differences in drug clearance. In contrast, some of these limitations can be overcome in a hollow-fibre system where multiple experiments can be performed more rapidly.⁶

Key characteristics of bacillary clearance for anti-TB drugs have been identified *in vitro* using the hollow-fibre infection model, such as a variable antimycobacterial effect of isoniazid over the course of treatment,⁷ and these findings correspond with *in vivo* antitubercular activity.⁸ These findings suggest not only that drugs may act on different parts of a cell, but that infections consist of different subpopulations of cells, which can have varying susceptibility to drugs. Most *in vitro* anti-tuberculosis studies use cfu and these data may not reflect the activity against susceptible, resistant or non-replicating bacterial subpopulations. Hence, attention is required to ensure accurate translation and interpretation of the results from such experimental protocols. Quantitative information on the number of respiring (alive) versus 'not respiring' (dead) cells and cells with damaged cell membranes (injured) or intact cell membranes using calcein violet and Sytox GreenTM staining methods can be a valuable tool and may provide insight into bacterial fitness.⁹

Parameterization of pharmacokinetic and bacillary killing data in PKPD models provides the possibility to interpolate and extrapolate bacillary clearance under different scenarios with the computer. Simulations to evaluate the appearance of persistent and tolerant bacterial subpopulations over the course of a treatment can provide crucial information.^{10,11} A variety of PKPD models have been developed to support antimicrobial drug combination research^{12,13} using *in vitro*,¹⁴ pre-clinical^{15,16} and clinical data.¹⁷ However, as for many other infectious diseases,^{18–22} rather complex model structures that include susceptible, resistant or non-replicating subpopulations have been used to parameterize bacillary clearance characteristics based on cfu data only.¹⁴ The concept of parameterizing the appearance of these subpopulations, i.e. bacterial fitness, into PKPD models is valid although it has to be data driven,²³ for example using data on bacterial fitness.

The aim of this investigation was therefore to demonstrate the potential of integrating both cell viability and cfu data in two separate PKPD models to complement the understanding of anti-bacillary effects of drug combinations using isoniazid/rifampicin and *Mycobacterium komossense* as a paradigm.

Materials and methods

Hollow-fibre model of infection

Isoniazid and rifampicin pharmacokinetic profiles in lung lesion homogenate, mimicking 600 mg and 300 mg daily oral doses of rifampicin (450 mg for patients <50 kg in body weight) and isoniazid, respectively, were

generated in the hollow-fibre model of infection. Drug levels generated in the hollow-fibre model of infection were also adjusted for protein binding, namely 42% for isoniazid and 83% for rifampicin (Table 1).²⁴ To ensure pharmacokinetic characteristics of the drugs were matched to the *M. komossense* growth characteristics, T_{max} and elimination $t_{1/2}$ were divided by three to adjust for the known differences in pathogen life cycle, i.e. 8 h versus 24 h for *M. komossense* and *Mycobacterium tuberculosis*, respectively.

A web application (https://pkpdia.shinyapps.io/hfs_app/) was used to convert adjusted secondary pharmacokinetic parameter estimates, C_{max} , T_{max} and $t_{1/2}$, into pump settings at a system volume of 133 mL (central reservoir, 75 mL; intracapillary space and tubing, 44 mL; and extracapillary space, 14 mL). Prior to T_{max} being reached, drugs were infused using a zero-order process into the central reservoir; thereafter flow rates between the diluent and central reservoir and central reservoir and elimination reservoir were set at an identical rate.

M. komossense (ATCC 33013) was incubated with Middlebrook 7H9 (Fluka) and 0.05% Tween (Sigma-Aldrich, UK) in sealed 50 mL tubes (Falcon, Corning, USA) at 30°C. This was done 3–5 days prior to inoculation of the hollow-fibre model of infection until OD₆₀₀>0.1. The hollow-fibre infection model was run at 30°C. The rifampicin experiments (at C_{max} =0.14, 0.4 and 1.47 mg/L with $t_{1/2}$ =1.57 h and τ =8 h) and the rifampicin/isoniazid experiment (at C_{max} rifampicin=0.4 mg/L and C_{max} isoniazid=1.2 mg/L with $t_{1/2}$ =1.57 h and τ =8 h) lasted for 7 days and the control experiments lasted for 10 days to ensure adequate characterization of the maximum carrying capacity. All experiments were performed as single runs and samples for bacterial load quantification and assessment of cell viability were taken every 24 h on weekdays. Drug concentrations in the hollow-fibre medium were not measured during the experiments.

Viable count measurement

Viable counts from daily samples from the hollow-fibre infection model were determined by cfu counts on Middlebrook 7H11 agar (Sigma-Aldrich, UK) as described previously.

Assessment of cell viability

M. komossense viability was assessed using Sytox GreenTM (Sigma-Aldrich) and resazurin sodium salt (alamar blue) (Sigma-Aldrich). Cultures were stained with resazurin at 0.01% solution overnight (16 h) in the dark and in the last hour of the incubation period Sytox GreenTM was introduced at 20 μM. Quantification was performed by flow cytometry using a Millipore Guava easyCyteTM HT system at 488 nm (blue light) and collected signal at 525/30 nm and 690/50 nm. Samples were loaded into a flat-bottomed 96-well plate (Nunc, Thermo Fisher, Denmark).

Modelling of cfu counts

A compartmental model using cfu data was fitted using NONMEM 7.3 on a Windows 10 operating system. Data were transformed into logarithm base 10 and minus twice the log likelihood of the data was used as objective function value (OFV). ADVAN9 and the FOCE-I method was used for estimation. Mean rifampicin population predictions were used as input for subsequent PKPD analysis.²⁵ Inclusion of one degree of freedom to a nested hierarchical model was considered to improve the model's ability to fit the data statistically if a drop in OFV of at least 3.84 ($P=0.05$) was achieved. Assessment of model performance was further supported by goodness-of-fit diagnostics.

Baseline bacterial load at experiment level (P_i) was estimated using typical baseline bacterial load (θ_{TV}) and a deviation from the typical baseline bacterial load for the rifampicin plus isoniazid experiment (COV) with a residual error term (e) (Eq. 1).

Table 1. Summary of pharmacokinetic settings for the hollow-fibre model of infection experiments

Parameter	Growth curve	Rifampicin			
		$C_{max} = 0.14 \text{ mg/L}$	$C_{max} = 0.4 \text{ mg/L}$	$C_{max} = 1.47 \text{ mg/L}$	Rifampicin $C_{max} = 0.4 \text{ mg/L} + \text{isoniazid}$ $C_{max} = 1.2 \text{ mg/L}$
Rifampicin $C_{T=2 \text{ min}}$ (mg/L)	—	0.00651	0.0186	0.0686	0.0186
Rifampicin C_{max} (mg/L)	—	0.14	0.400	1.47	0.400
Rifampicin AUC (mg·h/L)	—	0.317	0.905	3.34	0.905
Isoniazid C_{max} (mg/L)	—	—	—	—	1.20
Isoniazid AUC (mg·h/L)	—	—	—	—	2.73
T_{max} (h)	—	0.717	0.717	0.717	0.717
$t_{1/2}$ (h)	—	1.57	1.57	1.57	1.57
τ (h)	—	8	8	8	8

$C_{T=2 \text{ min}}$, predicted concentration 2 min after dosing; C_{max} , predicted maximum concentration; AUC, predicted AUC at steady-state; T_{max} , predicted time at which maximum concentration occurs; $t_{1/2}$, predicted elimination $t_{1/2}$; τ , dosing interval or time between dose administration.

$$P_i = 10^{\theta_{\text{IV}} \times (1+\text{COV}) + \epsilon} \quad (1)$$

Data from the growth control experiment was used to develop a log growth model (Eq. 2) using the parameters net growth ($\theta_{k_{net}}$) and maximum carrying capacity ($\theta_{cfu_{MAX}}$).

$$\frac{dcfu}{dt} = \theta_{k_{net}} \times cfu \times \log\left(\frac{10^{\theta_{cfu_{MAX}}}}{cfu}\right) \quad (2)$$

Data from the rifampicin therapy experiments were subsequently integrated into the analysis to describe the antimicrobial effect of rifampicin (E ; Eq. 3). Drug effects were parameterized in terms of a maximum drug effect ($\theta_{E_{MAX}}$) and potency, i.e. the concentration at which half-maximum inhibition ($\theta_{IC_{50}}$) is achieved, where C is the predicted mean rifampicin concentration in the medium.

$$E = \frac{\theta_{E_{MAX}} \times C}{\theta_{IC_{50}} + C} \quad (3)$$

The onset time of the rifampicin antimicrobial effect was rifampicin concentration-dependent (E_{LAG} ; Eq. 4) and this was parameterized by the time at which half-maximum inhibition ($\theta_{Time_{50}}$) was achieved, which is dependent on the rifampicin concentration that realizes half-maximum delay ($\theta_{LAG_{RIF_{50}}}$). C is the predicted mean rifampicin concentration and Time is observed time in hours.

$$E_{LAG} = \frac{Time^{20}}{Time^{20} + \left(\theta_{Time_{50}} \left(1 - \frac{C^{20} + \theta_{LAG_{RIF_{50}}}}{C^{20} + \theta_{LAG_{RIF_{50}}}}\right)\right)^{20}} \quad (4)$$

Parameters describing growth characteristics (Eq. 2), rifampicin drug effect (Eq. 3) and delay in rifampicin effect (Eq. 4) were fixed when data from the isoniazid plus rifampicin experiment were included for evaluation of the isoniazid/rifampicin interaction effect. The variable antimycobacterial effect over the course of treatment (E_{Cease}), after isoniazid inclusion in the rifampicin experiment, was parameterized using an exponential model with the parameter time to half-maximum drug effect inhibition ($\theta_{Time_{1/2}}$; Eq. 5).

$$E_{Cease} = 1 - \left(1 - e^{-Time_{1/2} \cdot \log(2)}\right) \quad (5)$$

Change in cfu over time was consequently parameterized as (Eq. 6):

$$\frac{dcfu}{dt} = (\theta_{k_{net}} - (E \times E_{LAG} \times E_{Cease})) \times cfu \times \log\left(\frac{10^{\theta_{cfu_{MAX}}}}{cfu}\right) \quad (6)$$

Residual variability (ϵ) departing from model predictions (IPRED) to observations (y) was additive on two-sided \log_{10} -transformed data (Eq. 7):

$$y = IPRED + \epsilon \quad (7)$$

Model parameters have been reported in their original form in the *Supplementary data* (available at JAC Online) and relevant model parameters have been converted from nmol/L to mg/L and reported in the manuscript tables and figures.

Cell viability data parameterization

An unordered multinomial response model was developed to parameterize *M. komossense* viability data using the software package NONMEM 7.3 on a Windows 10 operating system. The FOCE-I method was used for estimations and mean rifampicin population predictions were used as input for subsequent PKPD analysis. Goodness-of-fit diagnostics and the OFV, defined as minus twice the log likelihood of the summary statistics data, was used to discriminate between hierarchical models. A drop in OFV of at least 3.84 ($P = 0.05$) after inclusion of one degree of freedom was considered statistically significant and reflected an improvement of the model.

Baseline data samples were taken 2 min after drug was added to the hollow-fibre infection model. Treatment effect was described using a logistic regression model, in which the log ratio of the probabilities of being alive to injured (Eq. 8) and the log ratio of the probabilities of being dead to injured (Eq. 9) were derived. The relationship between the proportion of alive, injured and dead bacteria at baseline in the growth curve, low, medium and high rifampicin experiment (j) and baseline rifampicin levels (predicted at 2 min after start of the experiment) were estimated first. Serial samples from the growth curve and the low, medium and high rifampicin experiment were used during the analysis to characterize the effect of rifampicin exposure (AUC_{0-24}) over time on the log ratio of the probabilities of being alive to injured (Eq. 8) and the log ratio of the probabilities of being dead to injured (Eq. 9). Subsequently, serial samples from the isoniazid plus rifampicin experiment were analysed to characterize drug-drug interaction under the assumption of an additive covariate effect on the log ratio of the probabilities of being alive to injured (Eq. 8) and the log ratio of the probabilities of being dead to injured (Eq. 9), where Pr is probability.

$$\log\left(\frac{\Pr(\text{Alive})}{\Pr(\text{Injured})}\right) = \theta(1) + (\theta(2) + (\theta(3) \times C_{\text{Time}=2\text{ minutes}}))_{j \neq \text{growth control}} \\ + ((\theta(4) + (\theta(5) \times \text{AUC}_{0-24}))_{j=\text{rifampicin}} \\ \times \theta(6)_{j=\text{isoniazid+rifampicin}}) \times \text{Time} \quad (8)$$

$$\log\left(\frac{\Pr(\text{Dead})}{\Pr(\text{Injured})}\right) = \theta(7) + (\theta(8) \times C_{\text{Time}=2\text{ minutes}}) \\ + ((\theta(9) + (\theta(10) \times \text{AUC}_{0-24}))_{j=\text{rifampicin}} \\ \times \theta(11)_{j=\text{isoniazid+rifampicin}}) \times \text{Time} \quad (9)$$

Probability of cells in a sample being alive (Eq. 10), dead (Eq. 11) or injured (Eq. 12) can be derived as follow:

$$\Pr(\text{Alive}) = \frac{\Pr(\text{Alive})}{1 + \Pr(\text{Injured}) + \Pr(\text{Dead})} \quad (10)$$

$$\Pr(\text{Dead}) = \frac{\Pr(\text{Dead})}{1 + \Pr(\text{Injured}) + \Pr(\text{Alive})} \quad (11)$$

$$\Pr(\text{Injured}) = 1 - \Pr(\text{Alive}) - \Pr(\text{Dead}) \quad (12)$$

Considering that the summary statistics at each sampling timepoint were analysed and not the state of each individual bacterium, residual variability (ϵ), departing from model-predicted probabilities ($IPRED$) to the observed proportions (y) was additive in a logit transformation (Eqs 13–15). Residual variability was described as follow:

$$\phi_{TV} = \log\left(\frac{IPRED}{1 - IPRED}\right) \quad (13)$$

$$\phi = \phi_{TV} + \epsilon \quad (14)$$

$$y = \frac{e^\phi}{1 + e^\phi} \quad (15)$$

Model parameters have been reported in their original form in the [Supplementary data](#) and rifampicin concentrations were converted from nmol/L to mg/L for presentation in the manuscript Tables and Figures.

Results

cfu modelling

cfu data (Figure 1) were fitted using an empirical turnover model (Table S1, Figures S1 and S2) and the antibacterial effect of rifampicin was parameterized as an additive drug effect with IC_{50} at 0.00320 mg/L and E_{max} at 1.4. Rifampicin levels between 0.000823 and 0.411 mg/L resulted in substantial changes in bacterial killing, whereas rifampicin levels above 0.823 mg/L did not (Figure 2).

The predicted delay to the onset of rifampicin effect was dependent on rifampicin levels with $\theta_{LAG_{RIF50}}$ at 0.132 mg/L and $\theta_{Time_{50}}$ at 28.9 h (Table S1). Consequently, rifampicin levels of 0.165 mg/L or higher caused an almost immediate antibacterial effect whereas concentrations lower than 0.165 mg/L also showed antibacterial activity but the effect is predicted to occur at a later time after start of drug administration (up to ~ 30 h) (Figure 2).

Inclusion of isoniazid in combination with rifampicin caused the overall antibacterial effect to decrease with time. At 438 h

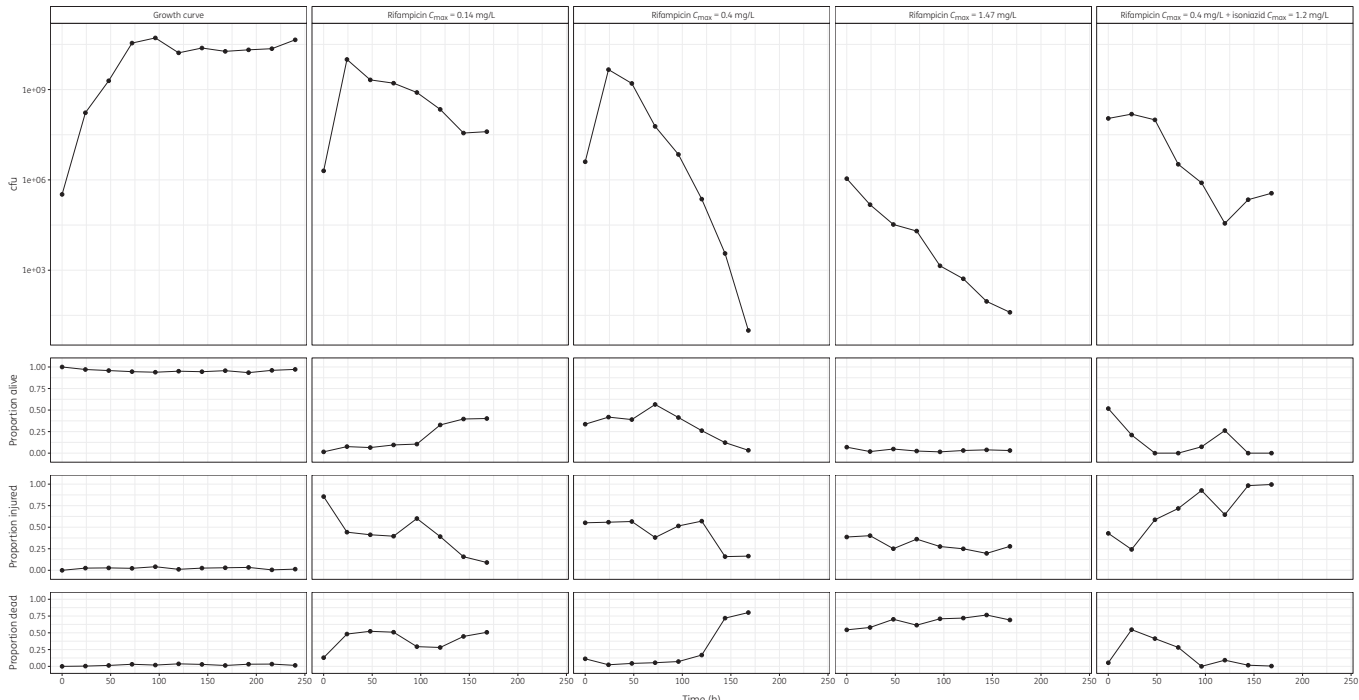


Figure 1. Visual representation of raw cfu-time data (top panels) and proportions of alive/injured/dead-time data (bottom three panels) for a growth curve experiment, a low ($C_{\text{max}} = 0.14 \text{ mg/L}$), medium ($C_{\text{max}} = 0.4 \text{ mg/L}$) and high ($C_{\text{max}} = 1.47 \text{ mg/L}$) rifampicin exposure experiment and a medium rifampicin exposure plus isoniazid experiment ($C_{\text{max rifampicin}} = 0.4 \text{ mg/L}$ and $C_{\text{max isoniazid}} = 1.2 \text{ mg/L}$). Dots represent observations and black lines are connecting lines.

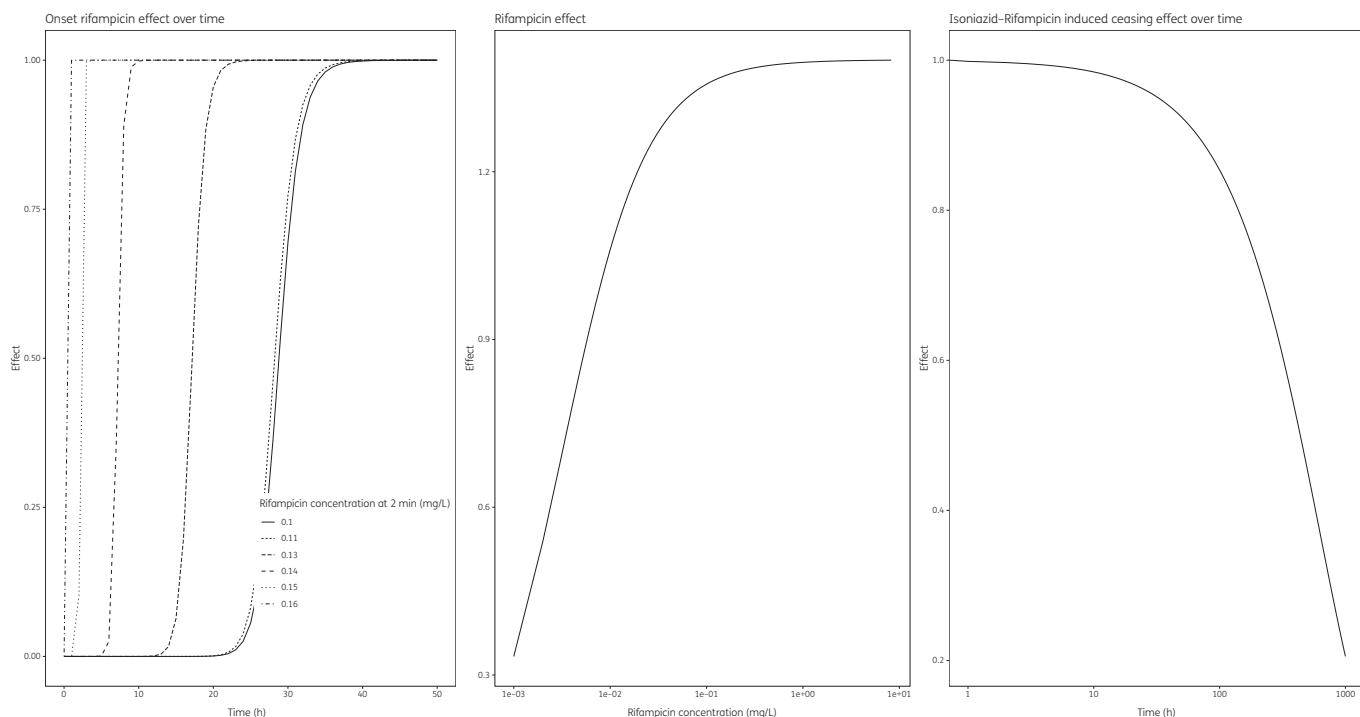


Figure 2. Visualization of drug effect characteristics in the differential equation model on cfu-time data. Rifampicin concentration-dependent effect onset (left panel), rifampicin effect (middle panel), and total isoniazid/rifampicin ceasing effect over time (right panel).

post-start of the experiment, half-maximum drug effect inhibition was reached (Table S1, Figure 2).

Cell viability data

Cell viability data (Figure 1) were fitted using an unordered categorical regression model (Table S2, Figures S3 and S4) and rifampicin exposure positively correlated with the proportion of dead cells over time (Figure 3). On the other hand, the probability of cells being injured or alive negatively correlated with rifampicin exposure over time (Figure 3).

Rifampicin also displayed distinct characteristics 2 min after the start of the experiment. Whilst a negligible proportion of the cells at baseline were injured or dead in the growth control experiment the proportion of alive cells dropped with increasing rifampicin concentration (Figure 3). Conversely, the proportion of dead cells increased with increasing rifampicin levels and the proportion of injured cells displayed an inverse quadratic relationship with rifampicin levels (Figure 3).

Other than when rifampicin was studied alone, inclusion of isoniazid in combination with rifampicin resulted in a decreased probability of alive and dead cells over time and an increased probability of injured cells over time (Figure 3).

Discussion

Understanding bacillary killing characteristics for antimicrobial drug combinations is both important and challenging. Historically, drug combinations, such as for the treatment of TB, have been selected based on empirical evidence and such a setting creates a

problem when one wants to identify novel combinations for both susceptible- and drug-resistant TB. The hollow-fibre infection model combined with live/dead staining techniques makes it possible to not only explore the antibacterial activity whilst taking into account the impact of different pharmacokinetic profiles, but also to integrate it with evolving technologies, which enable the characterization of phenotypes/subpopulations. Such an experimental setting offers a unique opportunity to evaluate antibacterial effects in a parametric manner, yielding estimates of antibacterial effects that can be compared across different compounds in a dose-independent manner. Such data provide the basis for the selection of compounds as well as further insight into the optimization of doses and dosing regimens.

Due to the complexity of bacillary killing data, often displaying biphasic elimination, assumptions about formation of susceptible, resistant or dormant bacterial subpopulations over time have been made^{14,17–22} without adequate data being available to support these hypotheses, resulting in identifiability problems.²³ Parameterization of staining data from bacterial samples such as proportion of alive/injured/dead cells over the treatment course in a logistic regression model can be a data-driven additional source of information to previously described models,¹⁴ providing a comprehensive insight into antimicrobial drug effects. However, for parameterization of this type of data a multinomial unordered logistic regression model should be used.

The rifampicin-driven bacillary killing displayed in the cfu data (Figure 2) coincided with the findings seen in viability data, in that the probability of cells being dead correlated positively with rifampicin AUC_{0-24} (Figure 3). The delayed onset of rifampicin-induced bacillary killing seen in the conventional cfu

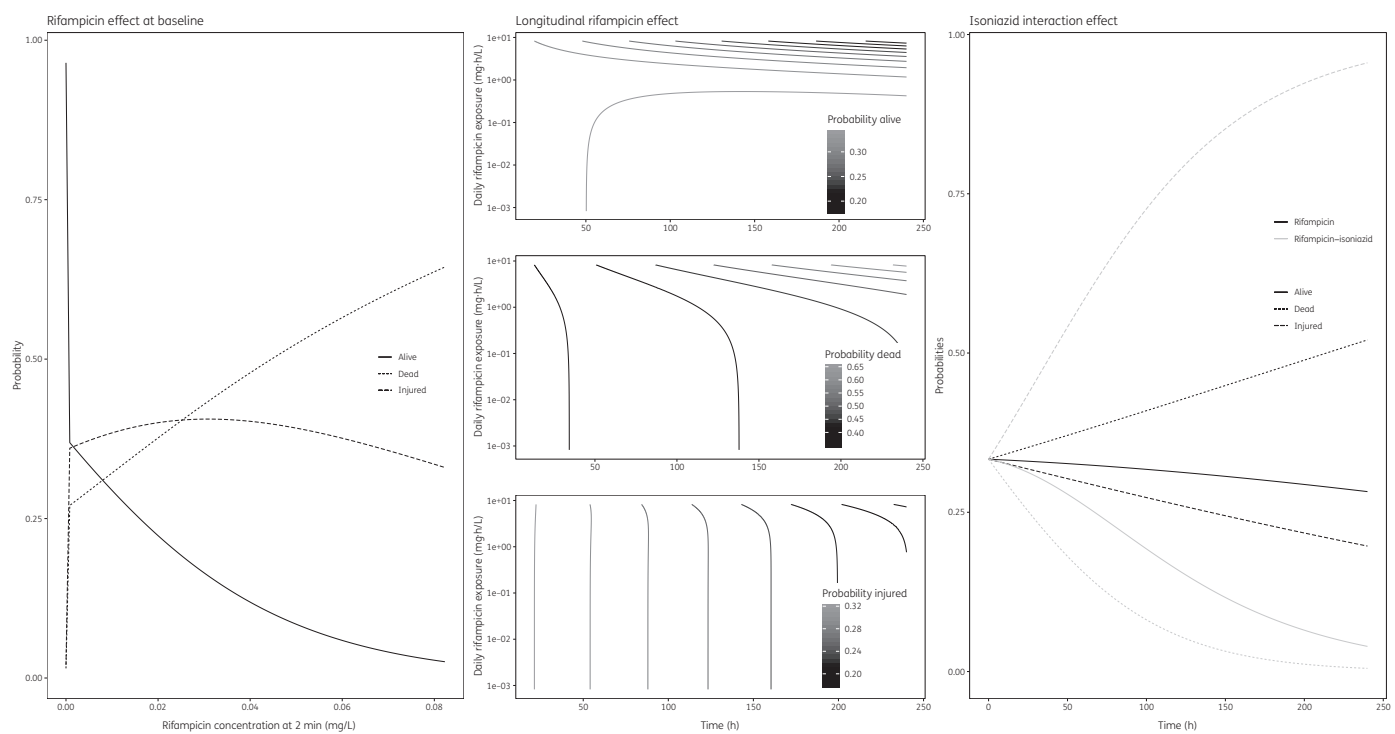


Figure 3. Visualization of drug effect characteristics in the multinomial regression model on bacterial viability–time data. Rifampicin-induced effect at baseline (left panel), rifampicin effect over time (middle panel) and total isoniazid/rifampicin effect over time (right panel).

data (Figure 2) coincided with the considerable proportions of injured and dead cells at baseline seen in viability data (Figure 3), in that increasing early rifampicin concentrations correlate negatively with time to bacillary killing onset and positively with the proportion of dead cells.

The delayed onset of rifampicin killing has not been previously reported, although published *in vivo*-mimicking hollow-fibre infection models for rifampicin used *M. tuberculosis*^{26–29} and the experiments presented here were performed with a different strain (*M. komossense*). Moreover, previous research simulated free rifampicin profiles in blood^{26–29} and these levels are higher compared with the free lung lesion homogenate exposures simulated in this study. The higher rifampicin levels in published research may explain the direct onset of rifampicin-driven antimicrobial effect.

The addition of isoniazid reduced rifampicin bacillary killing over time in the cfu data (Figure 2) and this coincided with an increased probability of injured cells over time at the cost of decreased probability of both alive and dead cells (Figure 3). The change in proportions of alive/injured/dead cells overlaps with previously reported ceasing isoniazid effect over the course of the treatment, which has been confirmed *in vivo* in patients and *in vitro* in a hollow-fibre infection model with *M. tuberculosis*.^{7,8} The latter study attributed this to the emergence of genotypic resistance.⁷ However, both experiments reported their findings based on isoniazid monotherapy and to the best of our knowledge this research describes the isoniazid–rifampicin interaction for the first time in an *in vitro* hollow-fibre infection model. These experiments should be replicated using *M. tuberculosis* to confirm the observations at varying isoniazid concentrations and higher rifampicin concentrations than

currently tested, alone and in combination. This will allow us to identify target exposure for the isoniazid/rifampicin combination that maximizes bacterial killing whilst minimizing the ceasing of the killing effect over time, which is key in light of current efforts to increase clinical rifampicin dosing.³⁰

The presented findings remain descriptive and are limited by the small sample size, and the impact of different experimental protocols has not been evaluated. Model parameterization is data driven and primarily aimed at describing the available data. The viability of cells in the hollow-fibre model of infection may need to be further characterized and different drugs and dosing regimens need to be tested to ensure the generalizability of the findings.

In summary, with the use of mathematical models becoming increasingly more common, we have shown that the evolution of bacterial viability over time can be fitted using empirical data-driven models. This type of data analysis, in addition to bacillary killing characteristics, can improve the understanding of the interaction of the moieties in a drug combination and provide the basis for hypothesis generation regarding treatment response in animal models and in humans. From a clinical microbiology perspective, addition of isoniazid reduced rifampicin bacillary killing over time in cfu data, coinciding with increased proportions of injured cells. Confirmation of these results using *M. tuberculosis* is required to establish the generalizability of the effect across different strains.

Acknowledgements

We would like to acknowledge the University of St Andrews for making the research facilities available.

Funding

This research was supported by a British Society for Antimicrobial Chemotherapy Research Grant (GA2015-172R). F. K. conducted the research as part of a Medical Research Council fellowship (MR/P014534/1). Neither the British Society for Antimicrobial Chemotherapy nor the Medical Research Council had a role in study design, data collection, analysis, decision to publish, or preparation of the manuscript.

Transparency declarations

O. D. P. is also Senior Director Clinical Pharmacology at GlaxoSmithKline. All other authors have none to declare.

Supplementary data

Tables S1 and S2 and Figures S1 to S4 are available as [Supplementary data](#) at JAC Online.

References

- 1** World Health Organization. Global Tuberculosis Report 2018. https://www.who.int/tb/publications/global_report/en/.
- 2** World Health Organization. Guidelines for treatment of tuberculosis 2010. <https://www.who.int/tb/publications/2010/9789241547833/en/>.
- 3** Fox W, Ellard GA, Mitchison DA. Studies on the treatment of tuberculosis undertaken by the British Medical Research Council tuberculosis units, 1946–1986, with relevant subsequent publications. *Int J Tuberculosis Lung Dis* 1999; **3**: S231–79.
- 4** Gillespie SH, Crook AM, McHugh TD et al. Four-month moxifloxacin-based regimens for drug-sensitive tuberculosis. *N Engl J Med* 2014; **371**: 1577–87.
- 5** Merle CS, Fielding K, Sow OB et al. A four-month gatifloxacin-containing regimen for treating tuberculosis. *N Engl J Med* 2014; **371**: 1588–98.
- 6** Cavaleri M, Manolis E. Hollow fiber system model for tuberculosis: the European Medicines Agency experience. *Clin Infect Dis* 2015; **61** Suppl 1: S1–4.
- 7** Gumbo T, Louie A, Liu W et al. Isoniazid's bactericidal activity ceases because of the emergence of resistance, not depletion of *Mycobacterium tuberculosis* in the log phase of growth. *J Infect Dis* 2007; **195**: 194–201.
- 8** Jindani A, Aber VR, Edwards EA et al. The early bactericidal activity of drugs in patients with pulmonary tuberculosis. *Am Rev Respir Dis* 1980; **121**: 939–49.
- 9** Hendon-Dunn CL, Doris KS, Thomas SR et al. A flow cytometry method for rapidly assessing *Mycobacterium tuberculosis* responses to antibiotics with different modes of action. *Antimicrob Agents Chemother* 2016; **60**: 3869–83.
- 10** Brauner A, Fridman O, Gefen O et al. Distinguishing between resistance, tolerance and persistence to antibiotic treatment. *Nat Rev Microbiol* 2016; **14**: 320–30.
- 11** Levin-Reisman I, Ronin I, Gefen O et al. Antibiotic tolerance facilitates the evolution of resistance. *Science* 2017; **355**: 826–30.
- 12** Brill MJE, Kristoffersson AN, Zhao C et al. Semi-mechanistic pharmacokinetic-pharmacodynamic modelling of antibiotic drug combinations. *Clin Microbiol Infect* 2018; **24**: 697–706.
- 13** Wicha SG, Chen C, Clewe O et al. A general pharmacodynamic interaction model identifies perpetrators and victims in drug interactions. *Nat Commun* 2017; **8**: 2129.
- 14** Clewe O, Aulin L, Hu Y et al. A multistate tuberculosis pharmacometric model: a framework for studying anti-tubercular drug effects *in vitro*. *J Antimicrob Chemother* 2016; **71**: 964–74.
- 15** Chen C, Ortega F, Rullas J et al. The multistate tuberculosis pharmacometric model: a semi-mechanistic pharmacokinetic-pharmacodynamic model for studying drug effects in an acute tuberculosis mouse model. *J Pharmacokinet Pharmacodyn* 2017; **44**: 133–41.
- 16** Chen C, Wicha SG, de Knecht GJ et al. Assessing pharmacodynamic interactions in mice using the multistate tuberculosis pharmacometric and general pharmacodynamic interaction models. *CPT Pharmacometrics Syst Pharmacol* 2017; **6**: 787–97.
- 17** Svensson RJ, Simonsson U. Application of the multistate tuberculosis pharmacometric model in patients with rifampicin-treated pulmonary tuberculosis. *CPT Pharmacometrics Syst Pharmacol* 2016; **5**: 264–73.
- 18** Bulitta JB, Yang JC, Yohonn L et al. Attenuation of colistin bactericidal activity by high inoculum of *Pseudomonas aeruginosa* characterized by a new mechanism-based population pharmacodynamic model. *Antimicrob Agents Chemother* 2010; **54**: 2051–62.
- 19** Landersdorfer CB, Ly NS, Xu H et al. Quantifying subpopulation synergy for antibiotic combinations via mechanism-based modeling and a sequential dosing design. *Antimicrob Agents Chemother* 2013; **57**: 2343–51.
- 20** Mohamed AF, Cars O, Friberg LE. A pharmacokinetic/pharmacodynamic model developed for the effect of colistin on *Pseudomonas aeruginosa* in vitro with evaluation of population pharmacokinetic variability on simulated bacterial killing. *J Antimicrob Chemother* 2014; **69**: 1350–61.
- 21** Nielsen EI, Viberg A, Lowdin E et al. Semimechanistic pharmacokinetic/pharmacodynamic model for assessment of activity of antibacterial agents from time-kill curve experiments. *Antimicrob Agents Chemother* 2007; **51**: 128–36.
- 22** Yadav R, Landersdorfer CB, Nation RL et al. Novel approach to optimize synergistic carbapenem-aminoglycoside combinations against carbapenem-resistant *Acinetobacter baumannii*. *Antimicrob Agents Chemother* 2015; **59**: 2286–98.
- 23** Jacobs M, Gregoire N, Couet W et al. Distinguishing antimicrobial models with different resistance mechanisms via population pharmacodynamic modeling. *PLoS Comput Biol* 2016; **12**: e1004782.
- 24** Lakshminarayana SB, Huat TB, Ho PC et al. Comprehensive physicochemical, pharmacokinetic and activity profiling of anti-TB agents. *J Antimicrob Chemother* 2015; **70**: 857–67.
- 25** Jacqmin P, Snoeck E, van Schaick EA et al. Modelling response time profiles in the absence of drug concentrations: definition and performance evaluation of the K-PD model. *J Pharmacokinet Pharmacodyn* 2007; **34**: 57–85.
- 26** Drusano GL, Neely M, Van Guilder M et al. Analysis of combination drug therapy to develop regimens with shortened duration of treatment for tuberculosis. *PLoS One* 2014; **9**: e101311.
- 27** Drusano GL, Sgambati N, Eichas A et al. The combination of rifampin plus moxifloxacin is synergistic for suppression of resistance but antagonistic for cell kill of *Mycobacterium tuberculosis* as determined in a hollow-fiber infection model. *MBio* 2010; **1**: e00139–10.
- 28** Gumbo T, Louie A, Deziel MR et al. Concentration-dependent *Mycobacterium tuberculosis* killing and prevention of resistance by rifampin. *Antimicrob Agents Chemother* 2007; **51**: 3781–8.
- 29** Srivastava S, Sherman C, Meek C et al. Pharmacokinetic mismatch does not lead to emergence of isoniazid- or rifampin-resistant *Mycobacterium tuberculosis* but to better antimicrobial effect: a new paradigm for antituberculosis drug scheduling. *Antimicrob Agents Chemother* 2011; **55**: 5085–9.
- 30** Svensson RJ, Svensson EM, Aarnoutse RE et al. Greater early bactericidal activity at higher rifampicin doses revealed by modeling and clinical trial simulations. *J Infect Dis* 2018; **218**: 991–9.